Available online at www.sciencedirect.com
ScienceDirect
Journal of Power Sources 175 (2008) 760–772
JOURNAL OF POWER SOURCES
www.elsevier.com/locate/jpowsour

Basic model for membrane electrode assembly design for direct methanol fuel cells

Ulrike Krewer, Hae-Kwon Yoon, Hee-Tak Kim *

Samsung SDI Co. Ltd., 575 Shin-dong, Yeongtong-gu, Suwon-si, Gyeonggi-do 443-391, Republic of Korea

Received 19 June 2007; received in revised form 21 September 2007; accepted 27 September 2007
Available online 13 October 2007

Abstract

This research proposes a model that predicts the effect of the anode diffusion layer and membrane properties on the electrochemical performance and methanol crossover of a direct methanol fuel cell (DMFC) membrane electrode assembly (MEA). It is an easily extensible, lumped DMFC model. Parameters used in this design model are experimentally obtainable, and some of the parameters are indicative of material characteristics. The quantification of these material parameters builds up a material database. Model parameters for various membranes and diffusion layers are determined by using various techniques such as polarization, mass balance, electrochemical impedance spectroscopy (EIS), and interpretation of the response of the cell to step changes in current. Since the investigation techniques cover different response times of the DMFC, processes in the cell such as transport, reaction and charge processes can be investigated separately. Properties of single layers of the MEA are systematically varied, and subsequent analysis enables identification of the influence of the layer's properties on the electrochemical performance and methanol crossover. Finally, a case study indicates that the use of a membrane with lower methanol diffusivity and a thicker anode micro-porous layer (MPL) yields MEAs with lower methanol crossover but similar power density.

Keywords: Direct methanol fuel cell; Parameter estimation; Operating conditions; Membrane; Diffusion layer; Power density

1. Introduction

The direct methanol fuel cell (DMFC) is seen as a promising power source for mobile electronic applications. However, major problems that cause low performance of the DMFC like high methanol crossover and low-methanol oxidation activity have not yet been solved. To improve DMFC performance, many experimental studies on the variation of material and layers inside the DMFC have been carried out [1–7]. These investigations have been matched by several works on modelling that mostly focused on the effect of specific materials and operating conditions on the DMFC. A recent review of DMFC modelling [8] categorises the model-based research.

A frequent approach to research on membrane electrode assembly (MEA) design concentrates on varying one layer and neglecting the effects of other DMFC layers on its performance. For a systematic approach to finding an optimum set of MEA materials, the screening of a large number of combinations of materials or layers would be required. Conducting such investigations experimentally is expensive and time-consuming. Therefore, a model-based performance prediction and optimization are of great interest for the MEA designer.

This research proposes an easily extendable DMFC MEA design model. Three main points lead to the MEA design model. First, a model is designed that is able to reproduce the experimental data. Parameters used in this design model are experimentally obtainable, and some of these parameters are indicative of material characteristics. The quantification of these material parameters builds up a material database. Second, processes in the DMFC such as transport, reaction and charge are separated, allowing their influence on the DMFC behaviour to be independently studied. This is undertaken by applying different investigative methods such as polarization, current-steps and electrochemical impedance spectroscopy (EIS), rather than using just a steady-state method (polarization) which contains the sum of all effects. Finally, the MEA layer properties are varied and key parameters for reproducing the features of each layer are identified.

* Corresponding author. Tel.: +82 31 210 7047; fax: +82 31 210 7374.
E-mail address: hee-tak.kim@samsung.com (H.-T. Kim).

0378-7753/$ – see front matter © 2007 Elsevier B.V. All rights reserved.
doi:10.1016/j.jpowsour.2007.09.115

Nomenclature

A_s	geometric electrode area of DMFC (m^2)
AW^{AD}	areal weight of anode diffusion layer ($g\,m^{-2}$)
c_{Pt}	active surface concentration of Pt (=0.117 $mol\,m^{-2}$)
c_{Ru}	active surface concentration of Ru (=0.165 $mol\,m^{-2}$)
$c^{A}_{CH_3OH}$	methanol concentration inside anode compartment ($mol\,m^{-3}$)
$c^{A,in}_{CH_3OH}$	methanol concentration of inlet feed ($mol\,m^{-3}$)
$c^{AC}_{CH_3OH}$	methanol concentration in anode catalyst layer ($mol\,m^{-3}$)
$c^{ADM}_{CH_3OH}$	methanol concentration at interface of anode diffusion layer and anode micro-porous layer ($mol\,m^{-3}$)
C^{AC}	anode double layer capacitance (=3348 $F\,m^{-2}$)
C^{CC}	cathode double layer capacitance (=907 $F\,m^{-2}$)
d^{AD}	diffusion layer thickness excluding MPL (m)
d^{AD}_{eff}	effective diffusion layer thickness excluding MPL (m)
d^{AMPL}	thickness of anode micro-porous layer (m)
d^{AD}_{hyd}	thickness of GDL governed by convective flow (m)
d^{M}	thickness of membrane (m)
D_{CH_3OH}	diffusion coefficient of methanol in water at 333 K (=$3.79 \times 10^{-9}\,m^2\,s^{-1}$)
$D^{M}_{CH_3OH}$	diffusion coefficient of methanol in membrane at 333 K ($m^2\,s^{-1}$)
F	Faraday constant (=96485 $C\,mol^{-1}$)
F^{A}	flow rate of flow entering anode compartment ($m^3\,s^{-1}$)
g_{CO}; (g_{OH})	inhomogeneity/interaction factor for Frumkin/Temkin adsorption on Pt = 11 and Ru = 0.43
i_{cell}	total cell current density ($A\,m^{-2}$)
k^{AD}	effective mass transport coefficient in anode diffusion layer ($m\,s^{-1}$)
k^{AMPL}	effective mass transport coefficient in anode micro-porous layer ($m\,s^{-1}$)
r_{Ai}	reaction rate for anode reaction step i ($mol\,m^{-2}\,s^{-1}$)
r_{A10}	reaction rate constant for anode reaction step 1 (=$1.6 \times 10^{-4}\,m\,s^{-1}$)
r_{A20}	reaction rate constant for anode reaction step 2 (=$7.2 \times 10^{-4}\,mol\,m^{-2}\,s^{-1}$)
r_{A20}	reaction rate constant for backward reaction of anode reaction step 2 (=$9.91 \times 10^{4}\,mol\,m^{-2}\,s^{-1}$)
r_{A30}	reaction rate constant for anode reaction step 3 (=0.19 $mol\,m^{-2}\,s^{-1}$)
r_C	cathode reaction rate ($mol\,m^{-2}\,s^{-1}$)
r_{C0}	cathode reaction rate constant (=$4 \times 10^{-6}\,mol\,m^{-2}\,s^{-1}$)
R	universal gas constant (=8.314 $J\,mol^{-1}\,K^{-1}$)
R_{el}	ohmic resistance of membrane ($\Omega\,m^2$)
t	time (s)
T	temperature of DMFC (=343 K)
U^{θ}_0	standard cell voltage (=1.213 V)
U_{cell}	cell voltage (V)
V^{A}	volume of anode compartment (m^3)
V^{AC}	volume of anode catalyst layer (m^3)
w^{AMPL}_{carbon}	carbon loading of micro-porous layer ($kg\,m^{-2}$)
$w^{AMPL}_{carbon,eff}$	effective carbon loading of micro-porous layer ($kg\,m^{-2}$)
x^{AD}_{PTFE}	PTFE content in anode diffusion layer (excluding MPL)
x^{AMPL}_{PTFE}	PTFE content in micro-porous layer

Greek symbols

α_{A2} (α_C)	charge transfer coefficient for anode reaction step 2 (cathode reaction), =0.5 (=0.18)
β_{CO} (β_{OH})	symmetry parameter for Frumkin/Temkin adsorption on Pt (Ru) (=0.5)
ε^{AD}	porosity of anode diffusion layer excluding micro-porous layer
ε^{AMPL}	porosity of micro-porous layer
η_A	anode overpotential (V)
η_C	cathode overpotential (V)
θ_{CO}	surface coverage of Pt with CO_{ads}
θ_{OH}	surface coverage of Ru with OH_{ads}
ρ_{carbon}	bulk density of carbon (=$1.7 \times 10^3\,kg\,m^{-3}$)
ρ_{PTFE}	bulk density of PTFE (=$2.19 \times 10^3\,kg\,m^{-3}$)
τ^{AMPL}	tortuosity of micro-porous layer

2. Experimental

2.1. MEA preparation

In-house MEAs used either Nafion 115 (DuPont) or hydrocarbon membranes. The catalyst was Pt–Ru (1:1) black (HiSpec 6000, Johnson Matthey) and Pt black (HiSpec 1000, Johnson Matthey) for anode and cathode, respectively. Various anode gas-diffusion layers (GDLs) (SGL carbon group) were used: 31BC, 31DC, 31BA and 35BC. They differed in poly(tetrafluoroethylene) (PTFE) content and micro-porous layer (MPL). For the cathode, 10DA or 35DC (SGL carbon group) were used; both GDLs contain 20 wt.% PTFE. On the surface of the 10DA cathode diffusion layer, a 1:1 (w/w) mixture of carbon (Vulcan XC-72, Cabot) and PTFE (DuPont) dispersed in isopropyl alcohol was applied in order to form a micro-porous carbon layer (MPL). The carbon loading of the MPL was controlled to be 1.3 $mg\,cm^{-2}$. Catalyst inks, which consisted of appropriate amounts of unsupported catalysts, Nafion 115 solution and isopropyl alcohol, were homogenized. The anode catalyst layer was prepared by spraying the ink on to the membrane. The Pt–Ru loading was 8 $mg\,cm^{-2}$, and the weight ratio of Nafion 115 to catalyst was 0.15. The cathode catalyst layer was prepared by spraying Pt-black ink on to the membrane. The layer had a mean Pt loading of 6 $mg\,cm^{-2}$ and the Nafion 115

to catalyst weight ratio was 0.16. The MEA was assembled by hot pressing the parts at 398 K and 500 kgf cm^{-2}.

The cell active area was either 10×10^{-4} m^2 or 26×10^{-4} m^2. The MEA was sandwiched between two plates with serpentine flow channels. Before recording any data, the cell was activated for several days.

2.2. Electrochemical characterization

All measurements were conducted with a Fuel Cell Test Station (Wonatech, Korea). For impedance measurements, an IM6 from Zahner Elektrik was used. Electrical heaters and a thermocouple were embedded in the bipolar plates for controlling the desired operating temperature of 343 K. A pump fed the anode with methanol solution.

On the anode, stoichiometric feed of methanol was provided. However, for current densities below 1000 A m^{-2} a minimum flow rate was applied; the minimum flow rate was adjusted to be identical to the stoichiometric flow rate at 1000 A m^{-2}.

During polarization, current step and mass balance experiments, the cathode was fed with air at atmospheric pressure at a constant flow rate of 500×10^{-6} m^3 min^{-1} (298 K, 10^{-5} Pa). During impedance measurements, hydrogen at a flow rate of 100×10^{-6} m^3 min^{-1} (298 K, 10^{-5} Pa) was fed to the cathode. During recording of the polarization curve, the current density was increased by 100 A m^{-2} every 70 s for low currents (<2 A); for higher currents, the current density was increased every 30 s by 200 A m^{-2}. Except for measurements close to the open-circuit voltage (OCV) at which the interaction of the adsorbed methanol intermediates may prevent a rapid establishment of a steady-state [9], the cell achieved a steady-state voltage within 10 s. For investigation of the cell voltage response to step changes in current, three different step changes were applied. Two were of equal step size with the first one in the low current density regime (1800 → 1000 A m^{-2}) and the second in the high current density regime (3800 → 3000 A m^{-2}). The third experiment was conducted in the low current density regime using a smaller step size (1800 → 1000 A m^{-2}). Each current was established for 3 min to guarantee that no interference between the single measurements would take place. The current step experiments were repeated three times. EIS were recorded at 1000, 2000 and 3000 A m^{-2} in a frequency range from 100 to 0.1 Hz. Measurements were performed under galvanostatic control of the cell. The amplitude of the sinusoidal voltage signal was 5 mV. The cathode acted as a reversible hydrogen electrode and the anode spectra were measured as a two-electrode set-up using the anode and the reversible hydrogen electrode. Mass balances were conducted to determine the methanol loss due to crossover. Balancing was done by measuring the mass change and concentration of the anode inlet and outlet flows, as well as the mass of water condensed at the cathode outlet, at which the flow was cooled to 273 K. The methanol concentration was determined by refractive index measurements using an Atago refractometer (RX5000α). The measurements were conducted over a time interval of 180 min at an anode and cathode flow rate of 3×10^{-6} and 500×10^{-6} m^3 min^{-1} (298 K, 10^{-5} Pa), respectively. Since methanol is volatile, this method may give results of medium accuracy. Alternative methods using CO_2 measurements for determination of crossover are given in [10,11].

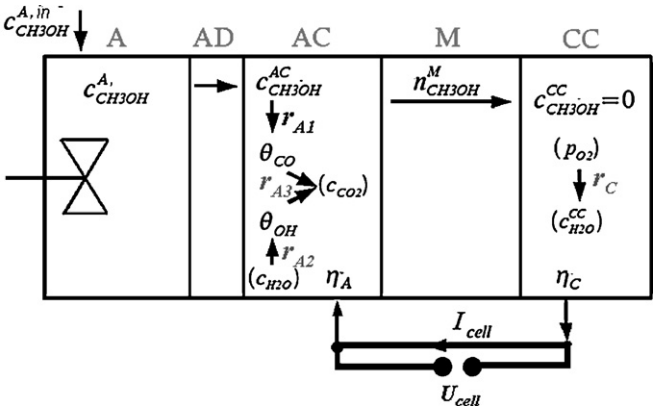

Fig. 1. Graphical representation of phenomena covered by DMFC model (terms in brackets are not taken into consideration).

3. Model

3.1. Model set-up

The DMFC model is a non-linear mathematical model that accounts for the following phenomena (see Fig. 1):

- diffusive mass transport of methanol through the anode diffusion layer,
- oxidation of methanol in the anode catalyst layer,
- formation of the intermediates CO (adsorbed on Pt) and OH (adsorbed on Ru) in the anode catalyst layer,
- electrochemical reduction of oxygen at the cathode catalyst layer,
- methanol crossover,
- undesired electrochemical oxidation of methanol at the cathode catalyst layer.

The model includes the following assumptions:

- ohmic drops in the current-collectors and electric connections are negligible,
- the fuel cell is operated isothermally,
- oxygen and carbon dioxide do not diffuse into the polymer electrolyte membrane (PEM),
- oxygen is fed in excess, i.e., oxygen conversion in the cathode compartment is negligible,
- the anode side water concentration is constant (excess component in a liquid mixture),
- on the anode side, a pure liquid phase mixture is assumed; CO_2 is postulated to dissolve instantaneously,
- the anode compartment is perfectly mixed,
- mass transport within the diffusion layers is fast, i.e., in a quasi-steady state,
- mass transport resistance in the catalyst layer is negligible,
- cathode side methanol reacts instantaneously with oxygen, i.e., its concentration on the cathode is zero,

- no pressure-driven transport through the membrane,
- electro-osmotic drag of methanol is negligible compared with methanol diffusive transport,
- mass transport in the membrane is in a quasi-steady state [9],
- a three-step reaction mechanism is used to describe the kinetics of the electrochemical oxidation of methanol [12].

The following set of equations holds for MEAs without an anode MPL:

$$\frac{\mathrm{d}c^{\mathrm{A}}_{\mathrm{CH_3OH}}}{\mathrm{d}t} = \frac{F^{\mathrm{A}}}{V^{\mathrm{A}}}(c^{\mathrm{A},in}_{\mathrm{CH_3OH}} - c^{\mathrm{A}}_{\mathrm{CH_3OH}}) - k^{\mathrm{AD}}\frac{A_{\mathrm{S}}}{V^{\mathrm{A}}}(c^{\mathrm{A}}_{\mathrm{CH_3OH}} - c^{\mathrm{AC}}_{\mathrm{CH_3OH}}) \quad (1)$$

$$\frac{\mathrm{d}c^{\mathrm{AC}}_{\mathrm{CH_3OH}}}{\mathrm{d}t} = k^{\mathrm{AD}}\frac{A_{\mathrm{S}}}{V^{\mathrm{AC}}}(c^{\mathrm{A}}_{\mathrm{CH_3OH}} - c^{\mathrm{AC}}_{\mathrm{CH_3OH}}) - \frac{A_{\mathrm{S}}}{V^{\mathrm{AC}}}\frac{D^{\mathrm{M}}_{\mathrm{CH_3OH}}}{d^{\mathrm{M}}}c^{\mathrm{AC}}_{\mathrm{CH_3OH}} - \frac{A_{\mathrm{S}}}{V^{\mathrm{AC}}}r_{\mathrm{A1}} \quad (2)$$

$$\frac{\mathrm{d}\theta_{\mathrm{CO}}}{\mathrm{d}t} = \frac{1}{c_{\mathrm{Pt}}}(r_{\mathrm{A1}} - r_{\mathrm{A3}}) \quad (3)$$

$$\frac{\mathrm{d}\theta_{\mathrm{OH}}}{\mathrm{d}t} = \frac{1}{c_{\mathrm{Ru}}}(r_{\mathrm{A2}} - r_{\mathrm{A3}}) \quad (4)$$

$$\frac{\mathrm{d}\eta_{\mathrm{A}}}{\mathrm{d}t} = \frac{1}{C^{\mathrm{AC}}}i_{\mathrm{cell}} + \frac{1}{C^{\mathrm{AC}}}(-4Fr_{\mathrm{A1}} - Fr_{\mathrm{A2}} - Fr_{\mathrm{A3}}) \quad (5)$$

$$\frac{\mathrm{d}\eta_{\mathrm{C}}}{\mathrm{d}t} = -\frac{1}{C^{\mathrm{CC}}}i_{\mathrm{cell}} - \frac{1}{C^{\mathrm{CC}}}6Fr_{\mathrm{C}} - \frac{1}{C^{\mathrm{CC}}}6F\frac{D^{\mathrm{M}}_{\mathrm{CH_3OH}}}{d^{\mathrm{M}}}c^{\mathrm{AC}}_{\mathrm{CH_3OH}} \quad (6)$$

$$r_{\mathrm{A1}} = r_{\mathrm{A10}}\exp[-\beta_{\mathrm{CO}}g_{\mathrm{CO}}(\theta_{\mathrm{CO}} - 0.5)]c^{\mathrm{AC}}_{\mathrm{CH_3OH}}(1 - \theta_{\mathrm{CO}}) \quad (7)$$

$$r_{\mathrm{A2}} = r_{\mathrm{A20}}\exp\left[\frac{\alpha_{\mathrm{A2}}F}{RT}\eta_{\mathrm{A}}\right]\exp[-\beta_{\mathrm{OH}}g_{\mathrm{OH}}(\theta_{\mathrm{OH}} - 0.5)](1 - \theta_{\mathrm{OH}}) - r_{\mathrm{A20}}\exp\left[-\frac{(1-\alpha_{\mathrm{A2}})F}{RT}\eta_A\right]\exp[(1-\beta_{\mathrm{OH}})g_{\mathrm{OH}}(\theta_{\mathrm{OH}} - 0.5)]\theta_{\mathrm{OH}} \quad (8)$$

$$r_{\mathrm{A3}} = r_{\mathrm{A30}}\exp[(1-\beta_{\mathrm{CO}})g_{\mathrm{CO}}(\theta_{\mathrm{CO}} - 0.5)]\theta_{\mathrm{CO}}\theta_{\mathrm{OH}} \quad (9)$$

$$r_{\mathrm{C}} = -r_{\mathrm{C0}}\exp\left[-\frac{(1-\alpha_c)F}{RT}\eta_c\right] \quad (10)$$

$$U_{\mathrm{cell}} = U^{\theta}_0 - \eta_{\mathrm{A}} + \eta_{\mathrm{C}} - R_{\mathrm{el}}i_{\mathrm{cell}} \quad (11)$$

Eq. (1) is the methanol mass balance in the anode compartment. Eqs. (2)–(4) are the mass balances of methanol, the intermediate CO and the intermediate OH in the anode catalyst layer. Eqs. (5) and (6) are the charge balances on the anode and the cathode sides, respectively. Eqs. (7)–(10) display the reaction rates at the anode and cathode. Finally, Eq. (11) describes the calculation of the overall cell voltage U_{cell}. A detailed variable and parameter notation is given in the nomenclature. In addition, Fig. 1 illustrates the phenomena covered by this set of equations and their interaction. If the diffusion layer contains a MPL, an additional description for this layer is required, since its properties differ strongly from that of the main GDL. As with the GDL, a quasi-steady state concentration profile is assumed in the MPL. The concentration at the interface between the GDL and MPL is denoted as $c^{\mathrm{ADM}}_{\mathrm{CH_3OH}}$, and the mass transfer coefficient for the MPL as k^{AMPL}. Eqs. (1) and (2) are replaced by the following:

$$\frac{\mathrm{d}c^{\mathrm{A}}_{\mathrm{CH_3OH}}}{\mathrm{d}t} = \frac{F^{\mathrm{A}}}{V^{\mathrm{A}}}(c^{\mathrm{A},in}_{\mathrm{CH_3OH}} - c^{\mathrm{A}}_{\mathrm{CH_3OH}}) - k^{\mathrm{AD}}\frac{A_{\mathrm{S}}}{V^{\mathrm{A}}}(c^{\mathrm{A}}_{\mathrm{CH_3OH}} - c^{\mathrm{ADM}}_{\mathrm{CH_3OH}}) \quad (12)$$

$$c^{\mathrm{ADM}}_{\mathrm{CH_3OH}} = \frac{k^{\mathrm{AD}}c^{\mathrm{A}}_{\mathrm{CH_3OH}} + k^{\mathrm{AMPL}}c^{\mathrm{AC}}_{\mathrm{CH_3OH}}}{k^{\mathrm{AD}} + k^{\mathrm{AMPL}}} \quad (13)$$

$$\frac{\mathrm{d}c^{\mathrm{AC}}_{\mathrm{CH_3OH}}}{\mathrm{d}t} = k^{\mathrm{AD}}\frac{A_{\mathrm{S}}}{V^{\mathrm{AC}}}(c^{\mathrm{ADM}}_{\mathrm{CH_3OH}} - c^{\mathrm{AC}}_{\mathrm{CH_3OH}}) - \frac{A_{\mathrm{S}}}{V^{\mathrm{AC}}}\frac{D^{\mathrm{M}}_{\mathrm{CH_3OH}}}{d^{\mathrm{M}}}c^{\mathrm{AC}}_{\mathrm{CH_3OH}} - \frac{A_{\mathrm{S}}}{V^{\mathrm{AC}}}r_{\mathrm{A1}} \quad (14)$$

The model should reproduce the polarization, EIS and current-step response experiments with one set of equations and parameters. All three-investigation methods use a change in cell current as an input for the experiment (Fig. 2). For steady-state investigations, the current is changed step-wise and only the respective steady-state voltage is recorded; the current step investigation evaluates the transient voltage response to a current step. Finally, in impedance spectroscopy, the current is varied sinusoidally, and the ratio between the voltage and current, i.e., the impedance, is recorded. For the steady-state and current step investigations, the set of equations can be used in its original form (Eqs. (1)–(14)). To model the recorded anode impedance spectra, the anode balance equations (Eqs. (2)–(5)) are transformed into the frequency domain. The detailed procedure of transformation has been explained in a previous study [12]. In contrast to modelling the EIS with equivalent circuit models, the model presented here has direct physico-chemical relevance, since it does not contain empirical elements. Furthermore, the equations and parameters are identical to that for steady-state and dynamic simulations.

3.2. Applied method of parameter identification

To determine a realistic parameter set for a given MEA, the effects of the various reaction and transport processes inside the MEA are separated and the characteristic parameters are identified. The motivation and procedure applied is as follows. A characteristic feature of each reaction, charge and transport process is its specific response time to changes in the state of the

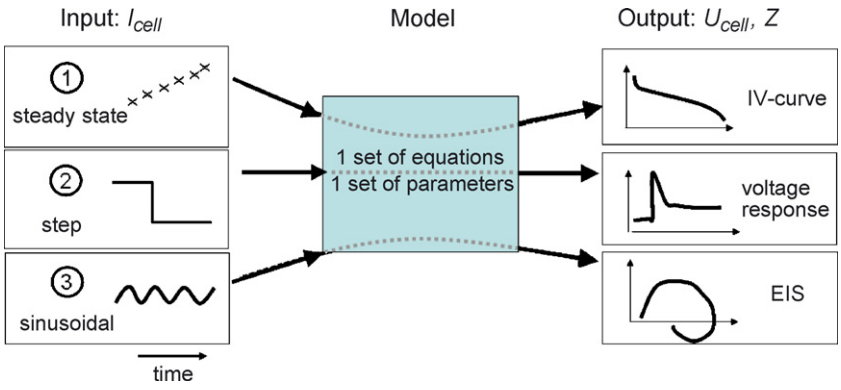

Fig. 2. Principle of modelling steady-state, dynamic and impedance measurements using one equation and parameter set.

MEA. Each process can therefore be attributed to an investigation method which covers the distinct time range of the process. The schematic in Fig. 3 illustrates that charge processes and fast kinetics influence the cell performance within seconds or milliseconds, while reactant/product transport or temperature change effects are observed over several seconds to minutes. In particular, the fast electrochemical processes at the electrode can be characterized with EIS. In previous studies of the response of DMFCs to step changes in current, it was found that a combination of fast kinetics and slow kinetics causes the experimentally observed strong voltage response. Transport processes such as methanol crossover contribute only a small additional effect after the main dynamic response has faded [9]. Finally, steady-state experiments like IV-measurements and mass balances are influenced by all processes in their steady-state. These experiments are especially useful to determine the transport parameters, since transport effects occur only after several seconds. They are barely covered by the other investigation methods.

For this research, the anode kinetic constants, capacitances and surface concentrations were approximated by fitting to anode impedance spectra and current step responses. R_{el} was determined from the anode EIS at high frequencies. GDL mass transport constants and membrane mass transport constants were fitted to polarization and mass balance experiments, respectively. Finally, the cathode reaction kinetic constants were approximated by fitting to the polarization curve.

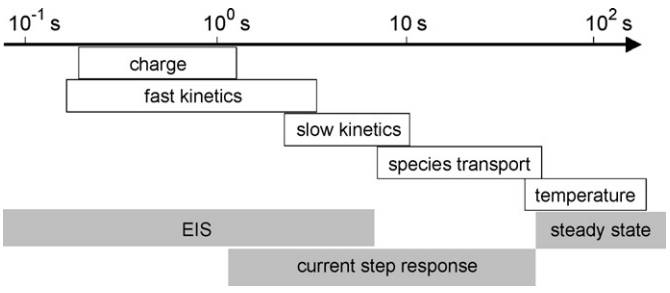

Fig. 3. Velocity of processes inside the DMFC and specific time range covered by experimental investigation methods.

4. Identification of anode kinetic parameters

In order to focus on the influence of the variation of the diffusion layer and membrane on a MEA's performance, one MEA was selected and the parameters related to its catalyst layer were identified. This MEA consists of Nafion 115, 31BC as anode GDL, the modified 10DA as cathode GDL (see Section 2.1), the standard cathode catalyst layer (see Section 2.1) and an anode catalyst layer of 6 mg cm^{-2} Pt–Ru loading with a Nafion/catalyst weight ratio of 0.07. The anode catalyst layer differs slightly from that used when conducting the diffusion layer and membrane transport parameter studies (Section 5), but the steady state and dynamic behaviour were very similar.

Since this work is conducted before an in-depth study of the effect of membrane and diffusion layers on MEA behaviour, the additional set of equations for a separate description for MPL and GDL was not taken into account, and literature-based transport parameters were used. The diffusion coefficient of methanol in Nafion 115 ($=6.26 \times 10^{-10}$ m^2 s^{-1}) was calculated using measurements presented by Kallio et al. [3]. The effective mass transport coefficient in the anode GDL ($=1.154 \times 10^{-5}$ m s^{-1}) was approximated by combining geometry and literature values as discussed in [9]. The anode flow rate was 10×10^{-6} m^3 min^{-1} and the active area was 10×10^{-4} m^2.

The kinetic parameters were fitted iteratively to the impedance spectra, current step experiments and anode and cell polarization experiments as motivated in Section 3. The impedance spectra were fitted roughly to identify a suitable range for the reaction rate constants and other parameters. It is assumed that the lumped description of the electrode and its structure may have prevented quantitative reproduction of the experiments. Nevertheless, the order of magnitude and ratio of the kinetic and charge parameters were identified (for parameter sensitivity see [12]). Simulation of the current step responses showed high sensitivity to the parameters of the slow reaction kinetics (r_{A10}, r_{A30}, g_{CO}, c_{Pt} and c_{Ru}), as predicted in Section 3, and this led to further refinement of the parameters.

The results of the parameter estimation are shown in comparison with the experimental results in Figs. 4–6. The IV-curve can be reproduced quantitatively (Fig. 4). Furthermore, the anode polarization curve was very close to the experimental one. The

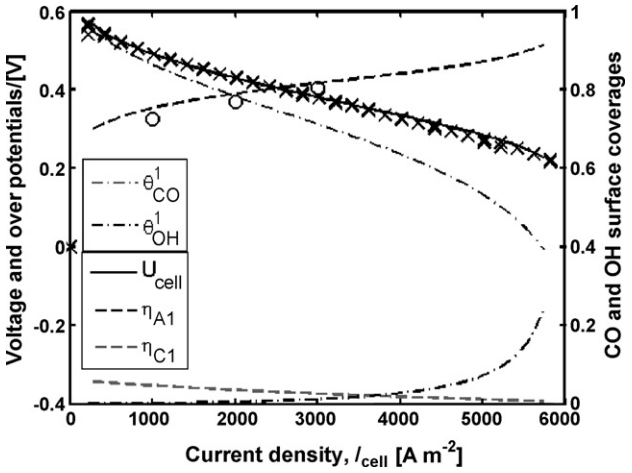

Fig. 4. Steady-state results: experimental (×) and simulated (–) steady-state IV-curve; experimental anode polarization (◯) and simulated overpotentials (—); surface coverages (–·–).

experimental data points of the latter were taken during the EIS measurements. The simulation result predicts the following contributions from the anode and the cathode sides:

- $i_{cell} < i_{cell,max}$: similar anode and cathode loss
- $i_{cell} \rightarrow i_{cell,max}$: anode-induced limitation (see θ_{OH} increase).

Fig. 5 shows that the model also quantitatively predicts the experimental dynamic behaviour of the DMFC to various step changes in current. Since the step response is governed by anode kinetics [13] and even the steady-state anode potential is reproduced (Fig. 4), a reasonable anode parameterization can be assumed. However, as explained before, the same parameter set did not yield a quantitative reproduction of the experimental anode EIS. This is shown in Fig. 6. While the shape and current level influence are qualitatively reproduced, the simulated curves are shifted to lower frequencies (Bode plot) and show

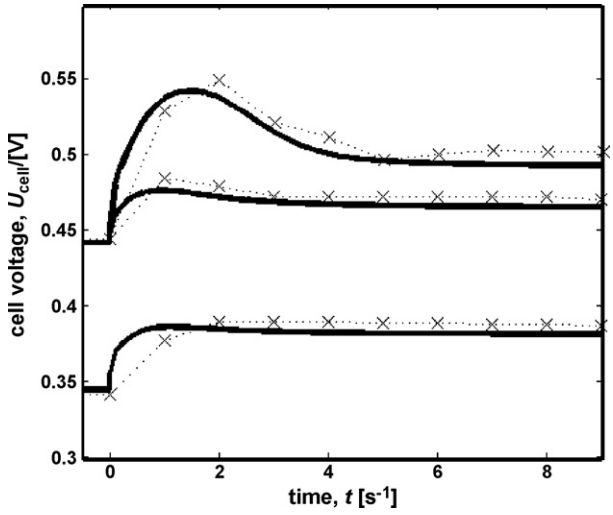

Fig. 5. Experimental (×) and simulated (–) response to cell current steps: 1800 → 1000 A m^{-2} (top), 1800 → 1400 A m^{-2} (middle) and 3800 → 3000 A m^{-2} (bottom).

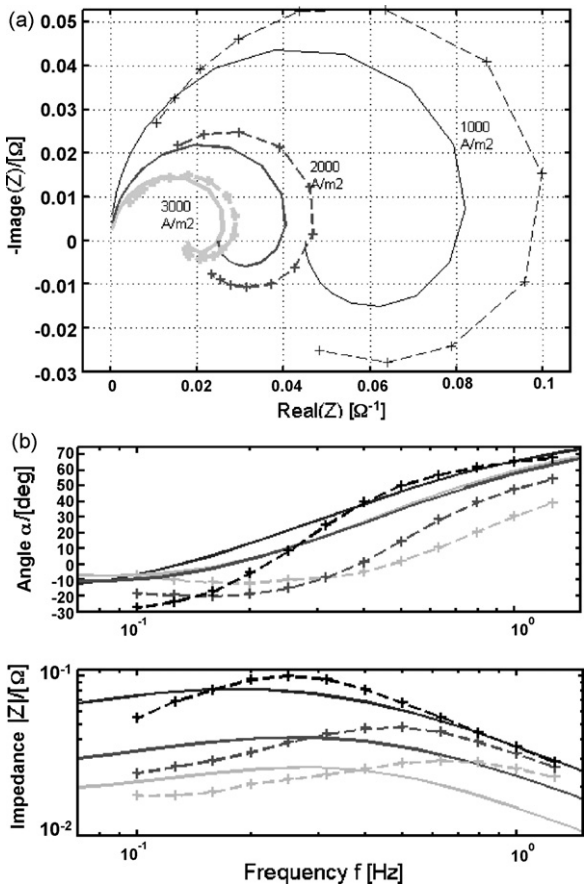

Fig. 6. Experimental (×) and simulated (–) electrochemical anode impedance spectra: 1000 A m^{-2} (black), 2000 A m^{-2} (grey) and 3000 A m^{-2} (light grey). (a) Nyquist plot and (b) Bode plot. Impedance spectra were corrected for ohmic drop.

a smaller dependence on the quasi-steady state cell current in comparison with the experiment (Nyquist and Bode plot).

5. Membrane and anode GDL key parameters

5.1. Membrane

Determination of the membrane and key GDL parameter values was done simultaneously. The GDL parameters used in this section for membrane characterization are those presented in Section 5.2 below.

The influence of the membrane on DMFC performance is twofold; ohmic resistance of the membrane R_{el} causes ohmic losses in the DMFC polarization curve and furthermore, methanol permeability of the membrane affects the polarization curve and Faradaic efficiency. The methanol permeability of a membrane depends on the membrane thickness d^M and on the diffusion coefficient of methanol in the membrane, $D^M_{CH_3OH}$. The contribution of electro-osmotic drag to the methanol crossover flux is small in the targeted low current density operating range. Also, the electro-osmotic drag would cause a positive deviation from the diffusion-induced linear decrease of crossover with current density. Such a positive deviation has not been observed in the literature [10,11]. Contributions by electro-

osmotic drag are therefore not accounted for by the model. Water permeability is an important issue [1,14] but it is not considered in this state of the MEA design model. The three parameters R_{el}, d^M and $D^M_{CH_3OH}$ cover the two main influences on the membrane, namely, electrical resistance and methanol crossover. They do not give a mechanistic explanation of the observed membrane behaviour, because such an approach is suitable for in-depth material specific studies but not for setting up a database consisting of arbitrary membrane materials, as targeted in this work. Instead, the user of the DMFC MEA design model should be familiar with all the parameters and be able to measure or estimate them easily. The membranes investigated and described here are a commercial Nafion 115 membrane and three hydrocarbon-based membranes; they are listed in Table 1.

Table 1
Key membrane parameters of the DMFC MEA model

Membrane	d^M (wet) ($\times 10^{-6}$ m)	R_{el} ($\times 10^{-4}\ \Omega\,m^2$)	$D^M_{CH_3OH}$ ($\times 10^{-10}\ m^2\,s^{-1}$)
N115	142	0.133	5
M1	43.2	0.065	1.45
M2	39	0.18	0.8
M3	41	0.13	1

For all membranes, the ohmic resistance of MEAs containing the respective membrane was measured by impedance spectroscopy at 343 K. It should be noted that these resistance values also contain a small contribution from the electronic resistances of

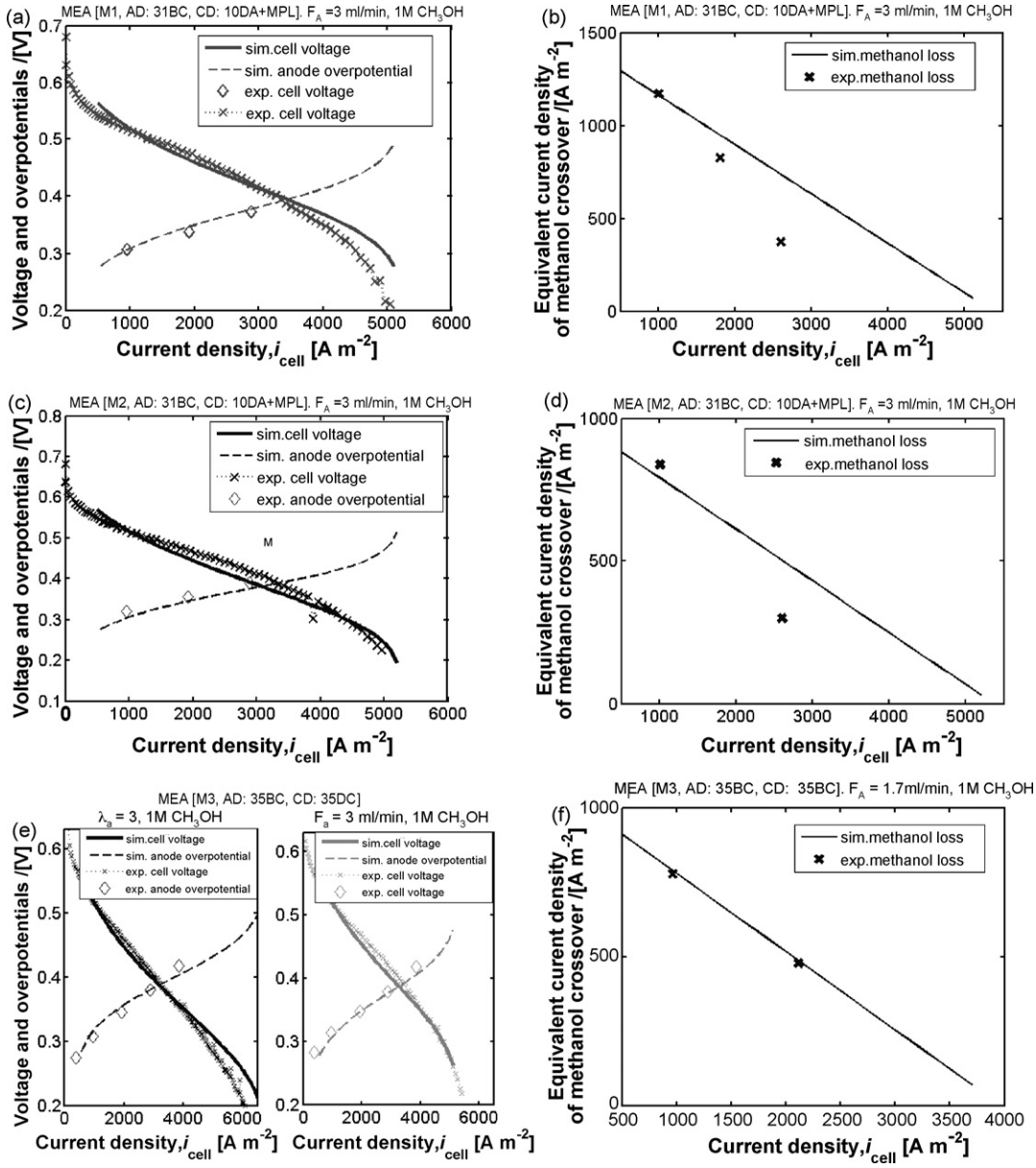

Fig. 7. Steady-state characterization of MEAs with membranes M1 (a and b), M2 (c and d), M3 (e and f). Left: polarization curve; anode overpotential. Right: equivalent current density loss by methanol crossover. MEA composition (AD: anode diffusion layer, CD: cathode diffusion layer) and operating conditions are given inside plots.

the respective MEA. The membrane thickness was measured experimentally after exposure to 1 M methanol solution. The diffusion coefficient was adjusted so that the simulated methanol crossover flux of the respective MEA matches the experimental one. A comparison of the experimental and simulated results is shown in Fig. 7 for MEAs containing the membranes M1, M2 and M3 and in Fig. 8 for various MEAs containing Nafion 115. The exact values of the key parameters for each investigated membrane are listed in Table 1.

5.2. Anode diffusion layer

Determination of the key parameters for the diffusion layer is more complex than that for the membrane. The effective methanol mass transport coefficient varies with PTFE content, porosity (or alternatively areal weight), thickness, and type of micro-porous layer (MPL) [2,15,16]. The existence or absence of an MPL significantly influences the mass transport to the anode catalyst layer, as shown in Fig. 8b and d; the MEA without MPL shows significantly higher methanol crossover (Fig. 8b) than the MEA with MPL (Fig. 8d). Influential MPL parameters are thickness, loading level and PTFE content. For a given MEA, the values for all six parameters are known or can alternatively be obtained by experiment. The PTFE content of GDL and MPL, GDL porosity, GDL/MPL combined thickness and MPL loading level are provided by the manufacturer. As an alternative to the GDL porosity, the GDL's areal weight can be measured. MPL and GDL thicknesses are obtained using a light microscope as shown in Fig. 9 (video microscope system Sometech SV 35). Microscopic pictures of the GDL/MPL 31DC show

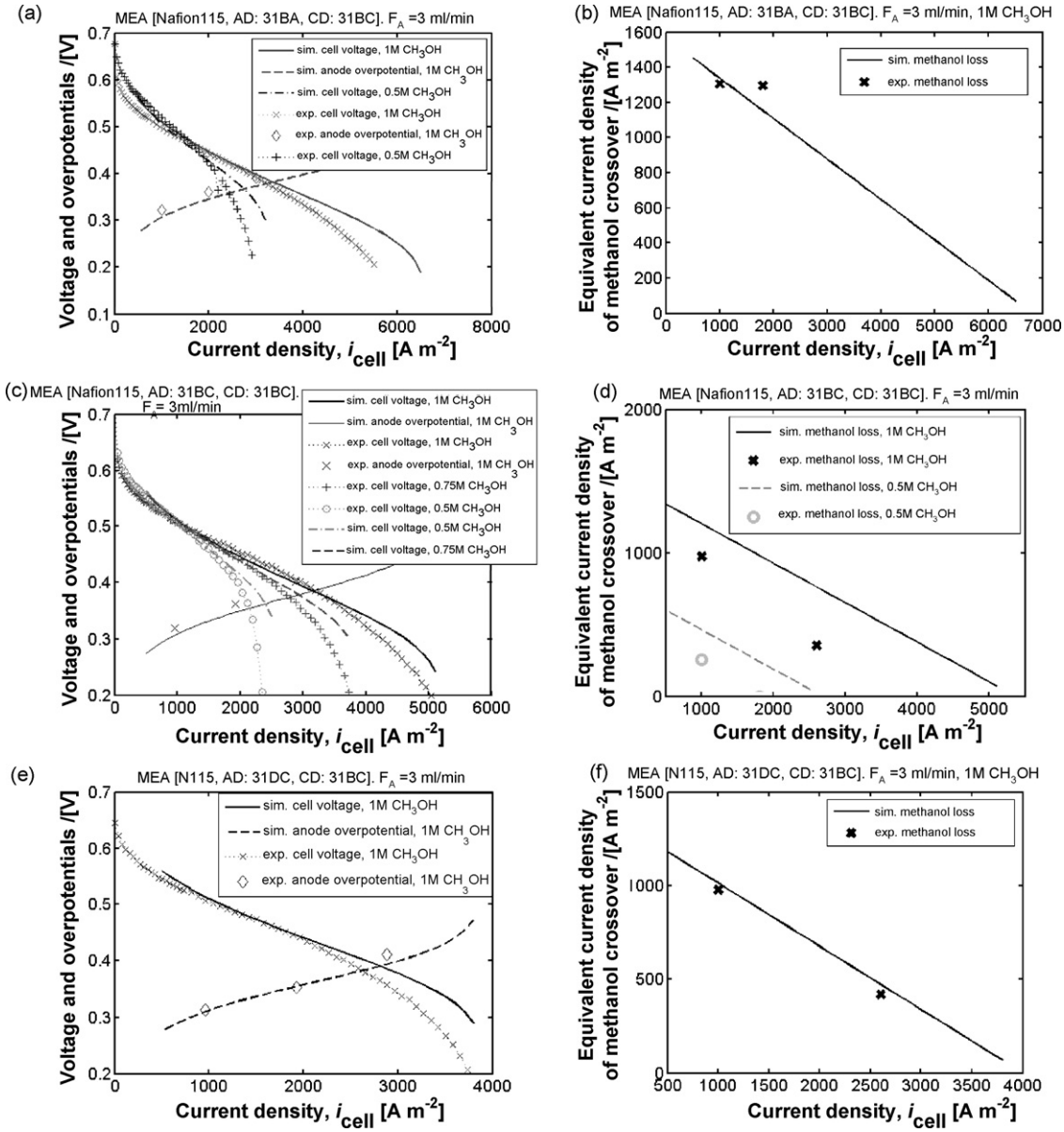

Fig. 8. Steady-state characterization of MEAs with Nafion 115 and various anode diffusion layers: 31BA (a and b), 31BC (c and d), 31DC (e and f). Left: polarization curve; anode overpotential. Right: equivalent current density of methanol crossover. MEA composition (AD: anode diffusion layer, CD: cathode diffusion layer) and operating conditions are given inside plots.

Table 2
Key parameters for diffusion layer and micro-porous layer (MPL)

Anode GDL and MPL	d^{AD} (excl. MPL) ($\times 10^{-6}$ m)	x^{AD}_{PTFE} (excl. MPL) (%)	AW^{AD} (excl. MPL) (kg m^{-2})	ε^{AD} (excl. MPL)	d^{AMPL} ($\times 10^{-6}$ m)	x^{AMPL}_{PTFE} (%)	w^{AMPL}_{carbon} (mg cm^{-2})
31BA	310	5	0.065	–	–	–	–
31BC	270	5	0.065	–	70	23	4
31DC	270	20	0.0743	–	70	23	4
35BA	295	5	0.0548	–	–	–	–
35BC	270	5	0.0548	–	70	23	4
35DC	239	20	0.0626	–	70	23	4
25BC	185	5	–	0.88	70	23	4
10DA + SDI MPL: 1.3 mg cm^{-2}	380	20	0.085	–	40	50	1.3

the GDL and MPL thickness (Fig. 9c) and highlight the strong structural differences between the porous GDL (Fig. 9a) and the dense MPL (Fig. 9b). An overview of the exact values of the key parameters for several GDL/MPLs is given in Table 2. In order to keep the DMFC MEA design model usable by many users as well as extendable for new materials, modelling of the diffusion layer is undertaken with only the above-mentioned key parameters as input parameters.

The diffusion layer mass transfer coefficient is calculated as follows:

$$k^{AD} = D_{CH_3OH}\frac{\varepsilon^{AD}}{d^{AD}_{eff}} \tag{15}$$

If the diffusion layer porosity ε^{AD} is not known, it is calculated by the experimentally measurable areal weight AW^{AD}, the PTFE content of the diffusion layer x^{AD}_{PTFE} and the bulk densities of the diffusion layer components carbon, $\rho_{carbon} = 1.7 \times 10^3$ kg m^{-3} and PTFE $\rho_{PTFE} = 2.19 \times 10^3$ kg m^{-3} [17]:

$$\varepsilon^{AD} = 1 - \frac{AW^{AD}}{d^{AD}}\left(\frac{x^{AD}_{PTFE}}{\rho_{PTFE}} + \frac{1 - x^{AD}_{PTFE}}{\rho_{carbon}}\right) \tag{16}$$

ρ_{carbon} was determined by applying Eq. (16) to a set of GDLs with 0 wt.% PTFE content (10AA, 31AA and 30AA) and matching the given values for AW^{AD}, d^{AD} and ε^{AD}.

An effective diffusion layer thickness d^{AD}_{eff}, which is based on the original key parameter d^{AD}, is introduced; d^{AD}_{eff} accounts for MEA compression and for the pressure-driven convective flow between adjacent anode channels through the GDL. According to Ref. [6], the pressure-driven convective flow through the GDL close to the anode flow-field ribs significantly increases methanol mass transport inside the diffusion layer. Also, calculations with the model presented above indicate that an additional transport phenomenon besides diffusion has to be present. When maximizing the DMFC model's GDL diffusion transport by setting the GDL porosity to 1 and keeping the original GDL thickness, the model predicts that the anode methanol concentration reaches 0 mol l^{-1} at current densities which are significantly lower than the experimentally obtained limiting current densities. To account for the pressure-induced convective transport, a hydrodynamic layer inside the GDL, which is governed by convective flow, is assumed. The layer decreases the real diffusion layer thickness to an effective value for diffusive mass transport, d^{AD}_{eff}. For a 50% compressed diffusion layer with 5 wt.% PTFE and thickness $d^{AD} > 280 \times 10^{-6}$ m, a constant thickness of the hydrodynamic layer ($d^{AD}_{hyd} = 60 \times 10^{-6}$ m) is identified, as explained in the discussion of Eq. (17). For thicknesses $d^{AD} < 280 \times 10^{-6}$ m, d^{AD}_{hyd} is assumed to decrease linearly to zero until $d^{AD} = 0$ m. In addition, the hydrodynamic layer inside the GDL depends on the PTFE content of the GDL. A high PTFE content increases GDL hydrophobicity and mechanically hinders convective flow due to formation of thin PTFE planes inside the GDL. Both effects should decrease the mass transport through the hydrodynamic layer. A linear influence of PTFE content on the hydrodynamic layer thickness is assumed. The effective diffusion layer thickness is then calculated as follows:

$$d^{AD}_{eff} = 0.5d^{AD} - d^{AD}_{hyd}\left(1 - \frac{x^{AD}_{PTFE} - 0.05}{0.2 - 0.05}\right) \tag{17}$$

Here 0.2 and 0.05 are the PTFE contents (wt.%) in the anode GDLs of the MEAs presented in Fig. 8. Validation of Eq. (17) was done using the experimental polarization curves presented in Fig. 8c and e. The experimental limiting current densities shown in Fig. 8c and e are strongly dependent on the PTFE content and are reproduced by the model for several concentrations. The dependence of methanol loss on concentration is also correctly predicted, but the experiment shows a lower actual effect of PTFE content on methanol crossover.

The MPL mass transfer coefficient is calculated as follows:

$$k^{AMPL} = D_{CH_3OH}\frac{\varepsilon^{AMPL}}{\tau^{AMPL}d^{AMPL}} \tag{18}$$

with the assumption

$$\frac{\varepsilon^{AMPL}}{\tau^{AMPL}} = (\varepsilon^{AMPL})^{1.5} \tag{19}$$

Here ε^{AMPL} is the MPL porosity, τ^{AMPL} the MPL tortuosity, and d^{AMPL} is the MPL thickness. Eq. (19) is used for micro-porous layers such as the catalyst layer or MPL. MPL porosity is calculated using the MPL key parameters:

$$\varepsilon^{AMPL} = \frac{d^{AMPL} - (w^{AMPL}_{PTFE}/\rho_{PTFE}) - (w^{AMPL}_{carbon,eff}/\rho_{carbon})}{d^{AMPL}} \tag{20}$$

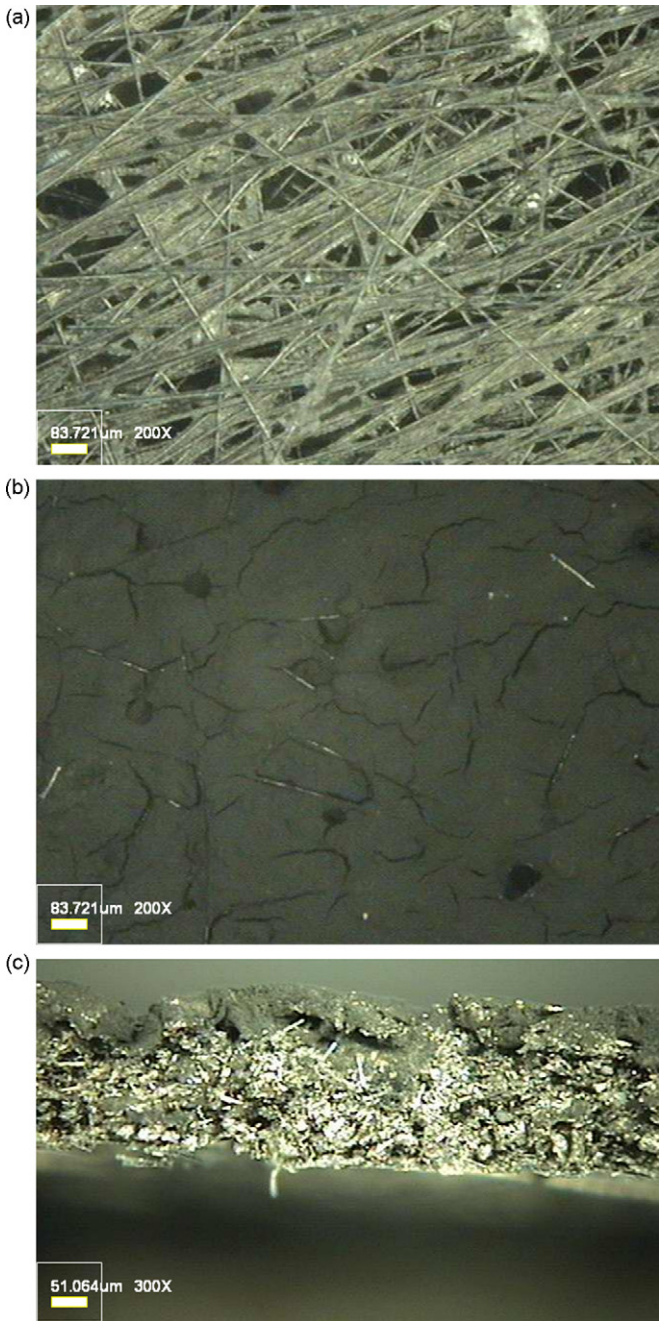

Fig. 9. Micrographs of GDL/MPL 31DC. (a) View of uncoated side of GDL/MPL, (b) view of MPL-coated side of GDL/MPL and (c) cross-sectional view of GDL/MPL with MPL on upper side.

where $w^{\mathrm{AMPL}}_{\mathrm{carbon,eff}}$ is the effective carbon loading of the MPL and $w^{\mathrm{AMPL}}_{\mathrm{PTFE}}$ the PTFE loading calculated from the PTFE mass fraction $x^{\mathrm{AMPL}}_{\mathrm{PTFE}}$:

$$w^{\mathrm{AMPL}}_{\mathrm{PTFE}} = w^{\mathrm{AMPL}}_{\mathrm{carbon,eff}} \frac{x^{\mathrm{AMPL}}_{\mathrm{PTFE}}}{1 - x^{\mathrm{AMPL}}_{\mathrm{PTFE}}} \tag{21}$$

Modelling of the MPL effect by using the original MPL key parameters requires some adjustments. An equivalent procedure had been introduced when modelling the GDL effect on DMFC performance with GDL key parameters. Using the original MPL loading and the MPL thickness determined by microscopy, the model predicts insufficient methanol diffusion. As a result, the simulated limiting current densities were significantly lower than the experimental ones. Discussion with MPL producers and analysis of micrographs indicate that not all the applied MPL material is located in the MPL layer. During the MPL manufacturing process, the macro-pore sized diffusion layer permits the transport of a certain amount of MPL material deep into the diffusion layer; some was even reported to have completely passed the diffusion layer. Comparing experimental and simulated results of MEAs with and without MPL (Fig. 8a–d) indicates that the effective carbon loading may be 60 to 100% of the original carbon loading. This value is assumed to depend on PTFE loading in the GDL since this will affect penetration of the MPL material into the GDL. The following equation is proposed for the effective carbon loading:

$$w^{\mathrm{AMPL}}_{\mathrm{carbon,eff}} = w^{\mathrm{AMPL}}_{\mathrm{carbon}} \left(0.6 + 0.4 \frac{x^{\mathrm{AD}}_{\mathrm{PTFE}} - 0.05}{0.2 - 0.05} \right) \tag{22}$$

Fig. 8a and b shows the performance of a MEA without MPL and Fig. 8c and d shows that of a MEA with an MPL. The predicted limiting current densities are close to those of the experiments. The concentration dependence is also correctly reproduced. Probably due to gaseous carbon dioxide blocking the methanol transport at high current densities, however, the experimental cell voltage is lower than that predicted; this holds also for the MEA with 20% PTFE content shown in Fig. 8e and f. Finally, comparing the simulation results of the diffusion layer and the influence of the membrane on the corresponding experimental results, as shown in Figs. 7 and 8, it can be concluded that the model, using a basic, experimentally oriented set of key parameters for the diffusion layer and membrane, is able to predict the performance of a variety of MEAs.

6. Case studies for membrane and diffusion layer design

Since high Faradaic efficiency is a crucial issue in designing DMFC systems, MEAs with minimized methanol crossover are highly advantageous. To quantify the effect of membranes on DMFC performance, a case study using existing membranes is presented in the following. Fig. 10 gives a comparison between the performance of an MEA containing one M3 membrane and an MEA containing a stack of two M3 membranes. As can be seen from Table 1, M3 already has a significantly lower methanol diffusion coefficient ($D^{\mathrm{M}}_{\mathrm{CH_3OH}}$) than Nafion 115. This positive material property is neutralized, however, by a much lower membrane thickness compared with Nafion 115, which leads to similar mass transfer coefficients ($D^{\mathrm{M}}_{\mathrm{CH_3OH}}/d^{\mathrm{M}}$) for both membranes. Using two membranes, or equivalently a membrane M3 with a double thickness, should decrease methanol crossover but will also increase ohmic resistance twofold. The simulations were done at a stoichiometric methanol feed of 2.5 and a methanol inlet concentration of 1 M. Fig. 10a shows that the MEA with two membranes has a slightly lower cell current density for DMFC operation at 0.45 V. The difference in electrochemical performance between both MEAs

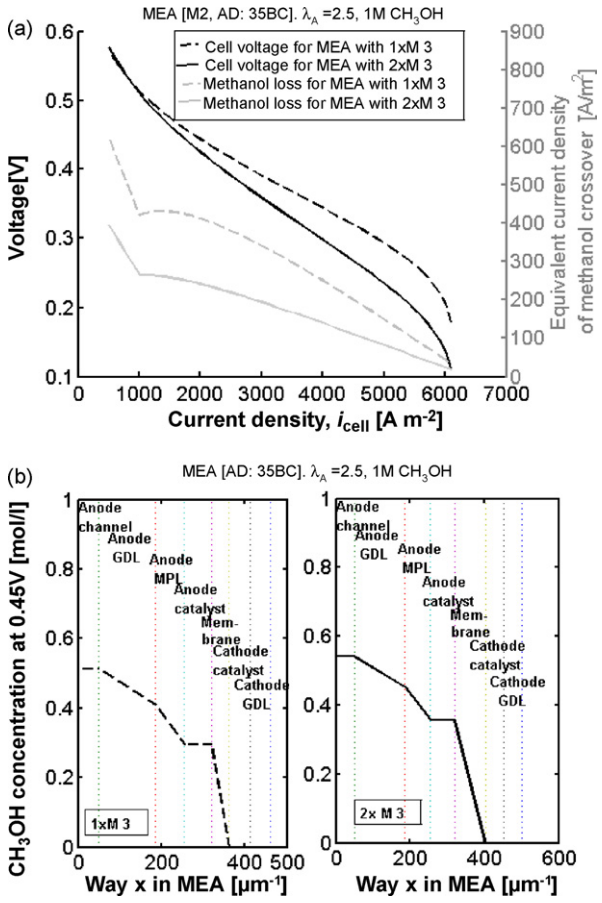

Fig. 10. Performance of MEA with one M3 membrane (dashed line) and with two M3 membranes (solid line) at anode stoichiometry 2.5. (a) Cell voltage (black) and methanol loss (grey). (b) Methanol concentration profile inside MEA. MEA composition (AD: anode diffusion layer) and operating conditions are given inside plots.

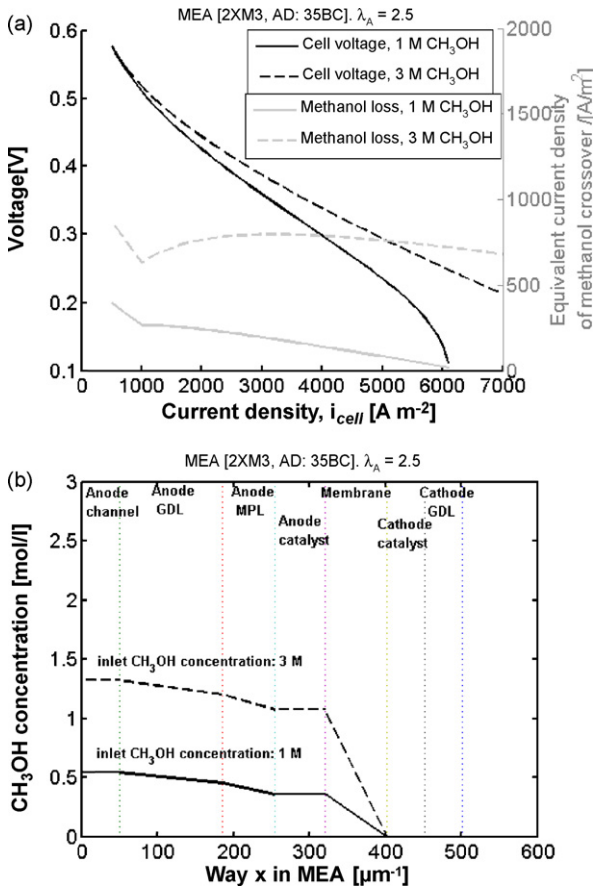

Fig. 11. Performance of MEA with two M3 membranes for 1 M CH_3OH (solid line) and for 3 M CH_3OH (dashed line) inlet concentration at anode stoichiometry 2.5. (a) Cell voltage and methanol loss. (b) Methanol concentration profile inside MEA.

increases to significant amounts for high current densities. While the MEA with two membranes shows a decrease in electrochemical performance as discussed, a 30% reduction in methanol crossover flux, is achieved. The proportional decrease in methanol crossover flux, which is achieved when using the MEA with two membranes, is similar for all current densities. By contrast, the difference between the absolute amounts of methanol lost by crossover becomes insignificant at high current densities. Fig. 10b shows the influence of the different membranes on the methanol concentration profile in the MEA. The MEA with two membranes significantly increases the mean methanol concentration level inside the anode catalyst layer and leads to a slight increase in methanol concentration even inside the anode channel. The low electrochemical performance at high current densities and the rather slight improvement in the corresponding crossover make the MEA with two membranes advantageous only for operation at low current densities and high cell voltages.

High anode flow rates correspond to high water loss and high electricity consumption by the feed pump; low anode flow rates may therefore be favourable for DMFC systems. If lower anode flow rates are used and the same anode feed stoichiometry is maintained, the inlet methanol concentration has to be increased. Fig. 11 shows a comparison of MEA performances at methanol inlet concentrations of 1 and 3 M; the MEA is the one discussed previously, with two M3 membranes and which shows improved performance in the high voltage region. Using inlet methanol concentrations of 3 M instead of 1 M leads to slightly increased electrochemical performances, but to greatly increased methanol crossover (Fig. 11a); methanol loss increases by more than twofold when using a 3 M methanol solution and is even higher than that for the MEA with a single M3 at 1 M (Fig. 10). Fig. 11b illustrates that the level of methanol concentration inside the MEA for 3 M inlet concentrations is between 1.5 and 1 M, in other words more than half of the original inlet concentration. The main reason for the increased methanol loss for the same stoichiometric flow rate is the transport of methanol inside the MEA driven by the concentration difference. It can be concluded that increasing membrane thickness is beneficial for DMFC operation at low current densities, while an increase of the inlet methanol concentration has a strongly negative impact on the Faradaic efficiency when operating at low current densities. This holds even for membranes with low methanol permeability.

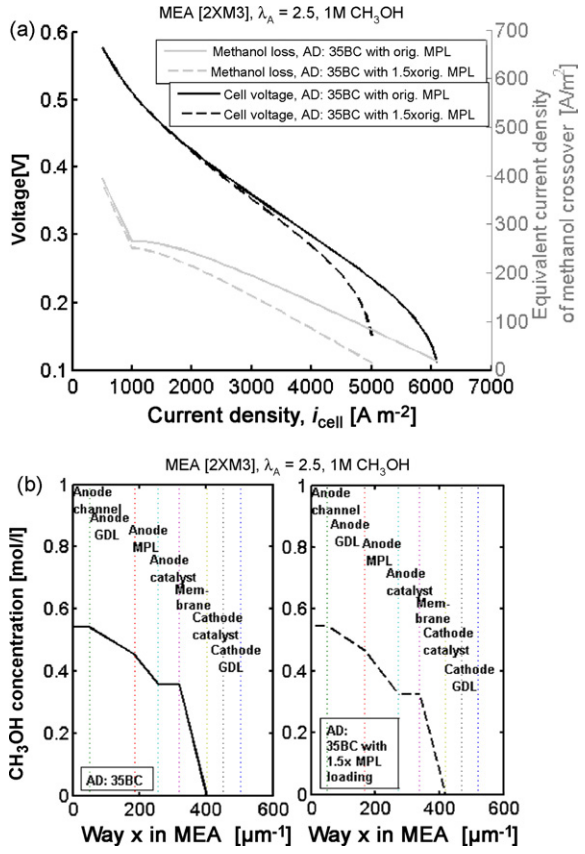

Fig. 12. Performance of MEA with modified anode MPL and two M3 membranes for 1 M methanol and anode stoichiometry 2.5: 35BC (solid line); 35BC + additional MPL (2 mg cm^{-2} carbon loading + 35 μm thickness increase). (a) Cell voltage and methanol loss. (b) Methanol concentration profile inside MEA.

A final case study should show the influence of increased MPL loading on performance. In order to increase further the performance of the MEA with two membranes (see Figs. 10 and 11), the MPL loading of the anode diffusion layer is increased 1.5 times. It is assumed that the MPL thickness also increases 1.5 times. The respective results are presented in Fig. 12. As shown in Fig. 12a, the MEA with the additional MPL loading displays the expected drop in limiting current density, whereas the electrochemical performance is essentially identical at 0.45 V and above. The methanol loss decreases for all current densities, but notably more at higher current densities. The methanol concentration profile at 0.45 V (Fig. 12b) illustrates the effect of the additional MPL loading. Due to a steeper concentration drop inside the MPL, the mean methanol concentration inside the anode catalyst layer decreases and causes less methanol crossover. It can be concluded that, when operating at 0.45 V, the MEA with additional MPL loading may be beneficial since it shows improved methanol efficiency while maintaining the same electrochemical performance.

7. Conclusions

This research proposes a DMFC MEA design model. The comprehensive model presented here is designed to be easily extendable so that additional phenomena can be incorporated at a later stage. Special attention is given to the selection of model input parameters which are easily obtained experimentally; this aspect facilitates building-up and future enlargement of the material database as well as extending the usability of the model.

For parameter identification, MEAs are investigated using different experimental methods such as polarization, current-steps and EIS. Since the experiments cover different response times of the DMFC, processes in the DMFC such as the transport, reaction and charge processes can be separately investigated. The main reaction kinetic parameters are identified at low current densities using anode EIS and current-step experiments. By systematic variation of the properties of the single layers inside the MEA, it is possible to identify key parameters for reproducing the influence of each respective layer on MEA performance. In this research, the basic structure of an extendable MEA design model is built up and variations of the properties of the anode diffusion layer and membrane are integrated. The model is presented with a basic, experimentally oriented set of key parameters and is able to predict the performance of a variety of MEAs.

Case studies for membrane and diffusion layer designs demonstrate the potential usefulness of the model for MEA design. The model predicts that increasing the membrane thickness decreases methanol crossover, especially at low current densities, while additional MPL loading decreases methanol crossover, especially at high current densities. For DMFC operation around 0.45 V, however, both modifications are beneficial for increasing the Faradaic efficiency while changes in the electrochemical performance are negligible. In contrast to these findings, operation at higher methanol concentrations at cell voltages of 0.45 V results in significantly increased methanol crossover. This increase is predicted to even neutralize the benefits obtained by improvements of the membrane or diffusion layer. For operation at high voltages, it is therefore recommended to adjust the inlet methanol concentration to around 1 M or less.

Acknowledgement

The authors are grateful to W.H. Jang for his global optimization tool which was used for EIS parameter fitting.

References

[1] R. Dillon, S. Srinivasan, A.S. Arico, V. Antonucci, J. Power Sources 127 (2004) 112–126.
[2] C. Xu, T.S. Zhao, Q. Ye, Electrochim. Acta 51 (2006) 5524–5531.
[3] T.V. Reshetenko, H.-T. Kim, U. Krewer, H.-J. Kweon, Fuel Cells 7 (2007) 238–245.
[4] T.V. Reshetenko, H.-T. Kim, H. Lee, M. Jang, H.-J. Kweon, J. Power Sources 160 (2006) 925–932.
[5] T. Kallio, K. Kisko, K. Kontturi, R. Serimaa, F. Sundholm, G. Sundholm, Fuel Cells 4 (2004) 328–336.
[6] G.Q. Lu, C.Y. Wang, J. Power Sources 134 (2004) 33–40.
[7] J.S. Cooper, P.J. McGinn, J. Power Sources 163 (2006) 330–338.
[8] V.B. Oliveira, D.S. Falcao, C.M. Rangel, A.M.F.R. Pinto, Int. J. Hydrogen Energy 32 (2007) 415–424.
[9] U. Krewer, K. Sundmacher, J. Power Sources 154 (2005) 153–170.

[10] R. Jiang, D. Chu, J. Electrochem. Soc. 151 (2004) A69–A76.
[11] S. Hikita, K. Yamane, Y. Nakajima, JSAE Rev. 22 (2001) 151–156.
[12] U. Krewer, M. Christov, T. Vidakovic, K. Sundmacher, J. Electroanal. Chem. 589 (2006) 148–159.
[13] U. Krewer, A. Kamat, K. Sundmacher, J. Electroanal. Chem. 609 (2007) 105–119.
[14] W. Liu, C.Y. Wang, J. Power Sources 164 (2007) 189–195.
[15] K. Scott, W.M. Taama, P. Argyropoulos, J. Appl. Electrochem. 28 (1998) 1389–1397.
[16] C. Lim, C.Y. Wang, J. Power Sources 113 (2003) 145–150.
[17] T. Schultz, Experimental and model-based analysis of the steady-state and dynamic operating behaviour of the direct methanol fuel cell (DMFC), PhD Thesis. University of Magdeburg, Magdeburg, 2005, http://diglib.uni-magdeburg.de/Dissertationen/2004/thoschultz.pdf.